EURASIAN JOURNAL OF MATHEMATICAL AND COMPUTER APPLICATIONS
ISSN 2306–6172
Volume 12, Issue 4 (2024) 75 – 83

AIR MASS MOVEMENT IN THE WIND TURBINES AREA AND ATMOSPHERIC BOUNDARY LAYER EVOLUTION WITH DISPERSED PHASE

Kovalnogov V.N., Fedorov R.V., Chukalin A.V., Demidov D.A., Kornilova M.I., Khakhalev Yu.A.

Abstract The numerical study results of the atmospheric boundary layer in the wind turbines area and atmospheric boundary layer evolution with precipitation in the STAR-CCM+ Academic Pack are presented. The numerical studies result of the dispersed phase influence on the velocity distribution in the wind turbine are presented. The flow velocity fields under different initial conditions are shown; flow rate of the dispersed phase (raindrops) and the particle sizes were varied. The obtained results will allow us to expand the theory of the turbulent wakes generation behind wind turbines. The presence of a dispersed phase in the air flow leads to a more rapid recovery of the wind turbine turbulent wake due to delay the particles by the flow and a reduction in the energy of turbulent eddies.

Key words:wind turbine, dispersed flow, atmospheric boundary layer, turbulent wake, mathematical modeling.

AMS Mathematics Subject Classification: 76F25.

DOI: 10.32523/2306-6172-2024-12-4-75-83

1 Introduction

At present, the widespread development of the wind energy industry can be seen, as noted by many analysts [1, 2]. Wind farms operate in a variety of weather and natural conditions, which has a significant impact on their efficiency and energy production. Researchers [3-5] studied the effect of precipitation on the wind turbines operation. The work [3] shows a reduction in wind turbine energy production due to rain of up to 20%, and due to wet snow of up to 36%. The power decreases for three reasons: the need for particles acceleration by the blades, the increase in weight and friction resistance of the blades due to particles sticking to them. The authors of [4, 5] investigated the effect of precipitation on blade erosion, and their results prove a decrease in the strength of wind turbine blades and, as a result, their service life. It can be noted that blade erosion leads to an increase in frictional resistance on their surface, which reduces their aerodynamic characteristics, and therefore the power generated.

With the development of wind energy, the role of predictive analytics is growing, which allows us to develop the most optimal recommendations for managing the wind turbines and wind farms operating modes. Today, such analytics cannot be imagined without mathematical and computer modeling of the atmospheric boundary layer in the wind turbines area. The mathematical description of the atmospheric boundary layer (ABL) in the wind farms area is complicated by the adequate representation of the boundary layer evolution taking into account the dispersed cluster (precipitation) [6-8].

2 Analysis of approaches and modeling methods

Currently, the study of dispersed flows with and without phase transitions is being carried out by leading scientific schools and laboratories in Russia, as well as China, Germany, Denmark, Great Britain, Israel, the USA and Japan [9-14]. The main difficulties in modeling two-phase turbulent flows are the turbulent nature of the flow and specific physical processes occurring in a dispersed turbulent flow: interaction of dispersed particles with turbulent eddies of the continuous phase; interaction of dispersed particles with each other as a result of collisions; evolution of the dispersed particles spectrum due to phase transitions, coagulation or fragmentation; the influence of turbulent fluctuations on phase transitions; interaction of particles with solid surfaces and deposition on them; the influence of dispersed particles on turbulence; diffusion, accumulation and fluctuations in the concentration of dispersed particles.

Modeling of two-phase flow involves modeling the mass, momentum, and heat transfer for each phase, as well as the interphase interactions. Mathematical models of two-phase flows can be divided into two-fluid and Euler-Lagrangian. The advantage of two-fluid models is the similarity of numerical models of dispersed flows with models of homogeneous flow, which allows the same numerical methods to be borrowed. A disadvantage of two-fluid models is the lack of information of the individual particles motion. The advantage of Euler-Lagrangian models is complete information about the motion of individual particles in the velocity and temperature field. The disadvantage of Euler-Lagrangian models is their resource intensity. In addition, if the concentration of the solid phase increases, the probability of particles colliding with each other increases, which complicates the trajectories calculation. When decreasing the particle size, it is necessary to take into account their interaction with small-scale turbulent structures, which also significantly complicates the calculation and requires more computing resources.

Many scientific papers present dispersed flows in straight channels with a constant cross-section, in which there is no inertial movement of particles in the boundary layer and their precipitation onto the surface [8-11]. However, the streamlined surfaces of wind turbines have a complex profile. Therefore, certain conditions are created that facilitate both the transverse movement of particles in the boundary layer and their inertial precipitation onto individual sections of the wind turbine blades surface when a dispersed flow moves. This leads to the intensification of exchange processes in the wind turbine area.

The analysis of the results presented in works [6-14] shows the following: a wide range of temperature changes in the plane-sections of a high-speed dispersed flow leads to the fact that dispersed particles can be in different phase states at different points; the movement of dispersed particles in high-speed dispersed flows is often accompanied by phase transitions such as crystallization, melting, condensation. In this case absorption or phase transition heat release and restructuring of the dispersed cluster occurs.

These features can have the largest influence on the intensity of exchange processes. Taking all this into account, the direct numerical solution to the system of differential equations of motion, continuity, energy and mass transfer for instantaneous values of flow parameters is a complex and resource-intensive task.

When using RANS models, including the Navier-Stokes equation system with Reynolds averaging and classical turbulence models, intense effects on the dispersed flow, such as pressure gradient or thermal and dynamic non-stationarity; redistribution of contribution of the pulsating velocity components to the kinetic energy of turbulence; non-monotonic change downstream of the kinetic energy of turbulent motion and the rate of its dissipation at the the boundary layer outer side of turbulent dispersed flows, are quite difficult to adequately

describe without simplifying assumptions, especially for wind farms [8-12]. The use of more complex multiparameter models of turbulent transport requires a significantly larger volume of empirical information, which is currently insufficient.

Currently, LES models are widely used [15]. LES models include filtered Navier-Stokes equations. They implement the principle of formal separation of large turbulent energy-carrying eddies and small formations due to high-frequency filtering applied to the Navier-Stokes equations. Large eddies are resolved explicitly by numerical simulations, and small-scale turbulence is parameterized, i.e. determined by the characteristics of large eddies [16].

Small-scale turbulence, where viscosity needs to be taken into account, can be described, for example, by the EVM (eddy viscosity models) or the Smagorinsky model [17-19]. The EVM approach has the ability to parameterize the direct energy transition from large to small eddies, but at the same time has a low correlation of the calculated stress tensor components with the experimental values of these components. Models based on the use of turbulent viscosity for turbulent eddies that cannot be resolved directly have become widely used [17]. The Smagorinsky model and its various modifications are also widely used, since it is quite simple and easy to implement [18, 19].

3 Physical problem, mathematical model and numerical research methodology

The ABL modeling in the wind turbine area was performed using the STAR-CCM+ CFD software [20].

Physical formulation of the problem: a non-stationary, turbulent, isothermal, two-phase flow of a viscous incompressible stream in a rectangular computational domain with an actuator disk simulating the operation of a wind turbine is considered. The length of the tunnel before the disk is 1400 m, after the disk – 2300 m. The radius of the actuator disk $R = 60$ m.

The thermophysical properties of the flow are constant: density $\rho = 1{,}176$ kg/m^3; kinematic viscosity $\nu = 1{,}576 \times 10^{-5}$ m^2/s; Prandtl number Pr = 0,712. The velocity profile at the inlet of the wind tunnel has a power-law dependence with an exponent 0,2, the maximum speed $u = 13$ m/s, at the hub of the wind turbine the speed is $u = 10$ m/s. The temperature is constant $T = 300$ K.

The thermophysical properties of the dispersed phase are also constant: density $\rho = 997{,}1$ kg/m^3; kinematic viscosity $\nu = 0{,}862 \times 10^{-6}$ m^2/s; Prandtl number Pr = 6,07. In the computational domain (wind tunnel), the injector is located on the top wall, the flow rate D of the dispersed phase is constant for each experiment, but changes in a series of experiments. The value of D is specified when describing the dispersed phase in the Lagrangian multiphase model before the calculation is performed. The dispersed phase size is also constant for each experiment, but changes in a series of experiments. The temperature is constant $T = 300$ K. The physical time of the experiment is 2000 seconds.

The eddy-resolving LES model was used to simulate the two-phase flow in the wind turbine area. The Navier-Stokes equations filtered by velocity components have the form: – continuity equation

$$\frac{\partial \bar{u}_i}{\partial x_i} = 0$$

– motion equation

$$\frac{\partial \bar{u}_i}{\partial t} + \bar{u}_j\left(\frac{\partial \bar{u}_i}{\partial x_j} - \frac{\partial \bar{u}_j}{\partial x_i}\right) = -\frac{1}{\rho}\frac{\partial \bar{p}}{\partial x_i} - \frac{\partial \tau_{ij}}{\partial x_j} + v\frac{\partial^2 \bar{u}_i}{\partial x_j^2} + \delta_{ijk} g \frac{\bar{\theta} - \langle \bar{\theta} \rangle}{\theta_0} + f_c \epsilon_{ijk} \bar{u}_j - \frac{f_i}{\rho}$$

– energy equation

$$\frac{\partial\bar{\theta}}{\partial t}+\bar{u}_j\frac{\partial\bar{\theta}}{\partial x_j}=-\frac{\partial q_i}{\partial x_j}+\alpha\frac{\partial^2\bar{\theta}}{\partial x_j^2}$$

where $\bar{u}_i$,$\bar{u}_j$ – filtered wind speed components, m/s; x_i,x_j– coordinates, m; ρ – density of the flow, kg/m^3; $\bar{p}$
– filtered pressure, Pa; ν – kinematic viscosity, m^2/s; g – acceleration of gravity, m/s^2; $\bar{\theta}$ – filtered temperature, $\langle\bar{\theta}\rangle$ – average filtered temperature, θ_0 initial temperature, K; f_c – Coriolis parameter; δ_{ijk} – variable unit tensor; α – thermal diffusivity of air, m^2/s; f_i
– aerodynamic drag force, kg×m/s^2; τ_{ij}, q_j –additional subgrid stresses, m^2/s^2, m×K/s, determined by formulas:

$$\tau_{ij}=\overline{u_iu_j}-\overline{u_i}\,\overline{u_j} \tag{1}$$

$$q_j=\overline{u_t\theta}-\overline{u_t}\overline{\theta} \tag{2}$$

Aerodynamic resistance f_i occurs as a result of the impact of wind turbine elements on a unit of air mass. It transforms the average kinetic energy of the incident flow and the energy of a large turbulent vortex into kinetic energy on the scale of wind turbine elements.

The tensors in equations (1) and (2) describe the influence of small-scale eddies on the evolution of large-scale eddies and need to be modeled.

In the proposed study, the Smagorinsky model was used. It describes the influence of small-scale eddies on the evolution of large-scale ones by the expression:

$$\tau_{ij}=-\frac{1}{3}\delta_{ij}\tau_{kk}\approx\tau_{ij}^{smag}=-2C_s^2\Delta_g^2|\overline{S}|\overline{S}_{ij},$$

where C_s – Smagorinsky constant, $\Delta_g=h$ – model grid step (if the grid step in different directions is different, then $\Delta_g=(h_xh_yh_z)^{1/3}$, $|\overline{S}|=\sqrt{2\overline{S}_{ij}\overline{S}_{ij}}$ – norm of the strain rate tensor, $C_s\Delta_g$ – length scale that can be interpreted as a mixing length l for subgrid scale vortices.

In accordance with [21], the Smagorinsky constant was taken $C_s=0{,}17$ and $Pr_T=0{,}4$. An actuator model of a wind turbine was used to simulate the wind turbine in order to save computational resources, since with this approach the full-scale geometric model is replaced by a disk simulating the impact of the wind turbine on the ABL. The STAR-CCM+ package provides the ability to use the "Virtual Disk" tool.

The motion of dispersed particles in the flow was modeled using the Lagrangian Multiphase model.

The equation for momentum conservation of a dispersed particle (drop) is written as:

$$m_L\frac{du_{Li}}{dt}=F_D+F_{PG}+F_{SL}+F_g=\sum_i F_i,\qquad m_L=\frac{\rho_L\pi d^3}{6}. \tag{3}$$

where ρ_L – density, kg/m^3; d – drop diameter, m; forces acting on drops: F_D – aerodynamic drag force, N; F_{PG} – force equivalent to the pressure gradient of the carrier medium, N; F_{SL} – radial force, N; F_g – gravitational force, N; Subscript $_L$ refers to a drop; u_{Li} – instantaneous velocity of a drop, m/s.

The force of aerodynamic drag is defined as $F_D=\frac{1}{2}\rho C_D(\pi d^2/4)(u_i-u_{Li})|u_i-u_{Li}|$ where C_D – drop drag coefficient.

Simcenter STAR-CCM+ provides several methods for determining the drag coefficient. In this work the Schiller-Naumann method [22] was used, according to which the drag coefficient of a drop is determined as $C_D=24\left(Re_L^{-1}+0,15Re_L^{-1/3}\right)$ where Re_L – Reynolds number for a drop, determined by the formula $Re_L=(u-u_L)d/v$.

The force equivalent to the pressure gradient of the dispersed flow is determined by the expression $F_{PG} = \rho\frac{\pi d^3}{6}\frac{Du}{Dt}$.

The radial force is determined from the expression $F_{SL} = 1,615\, d^2\rho(u-u_L)\sqrt{v\left|\frac{du_i}{dx_i}\right|}$; the force of gravity is determined according to the expression $F_g = m_L g(1-\rho/\rho_L)$. Under the forces, listed above, in the Lagrangian model the variables, describing the state of the particle, change in space and time, while the Euler fields are frozen.

The position and velocity of the particle are obtained by numerically integrating over time the particle momentum equation (3) and the position equation $\frac{dr_L}{dt} = U_L$, where r_L – instantaneous position vector.

Thus, the trajectory of a particle is a geometric locus of points obtained by integrating the equation of position.

In the statistical Lagrangian approach, packets of individual particles are tracked. A single state integration is applied to all particles in the packet, and any exchange with the Euler phase is multiplied by the number of particles in the packet.

The values of the continuous phase in the integration section are determined at the center of the cells, but the intermediate values of the continuous phase velocity are interpolated between the cell centers. Thus, the velocity is the only interpolated value of the continuous phase.

4 Numerical study and its results

In this study of the ABL in the presence of precipitation, the size of the dispersed phase (rain particles) changed d = 1 mm; 2,5 mm and volumetric flow rate D = 3,7 mm/h; 5,3 mm/h respectively, what can be imagined as light and moderate rain.

The falling speed of rain particles was determined by the formula [23]:

$$u_T = 9,58\left[1-\exp\left\{-\frac{d^{-1,147}}{1,77}\right\}\right]$$

The modeling was carried out on a scale of 1:1. Length of the computational domain l = 3700 m, width b = 400 m, height H = 500 m. Actuator disc diameter – 120 m. Initial turbulence intensity 0,02 was taken based on weather conditions, corresponding to light gusts of wind; The scale of the turbulence length was taken to be equal to 0,084 m.

The LES approach places special demands on the quality of the mesh. The polyhedral mesh included 9 348 564 cells with prismatic layers near the impermeable walls. The basic cell size of the calculation grid was 1 m; in the area of rotation of the wind wheel, the grid size was set at 0,05 m. In the wind turbine area, a mesh treatment was used (Fig. 1).

Based on the results of the numerical study, the velocity fields in the wind tunnel are obtained and presented in Fig. 2. Using the built-in STAR CCM+ tools, velocity profiles were constructed along the tunnel at a level of 100 m from the bottom wall (see Fig. 3). During the experiments, flows with different dispersed phases (presence and absence of particles, their size and flow rate) were considered.

Fig. 2 shows the results of the velocity field for air flow around a wind turbine. When examining the velocity field in front of a wind turbine, one can notice a change in the velocity amplitude caused by the initial turbulence of the air flow. The near wake behind the actuator disk is characterized by a significant decrease in velocity, with a decrease in speed to 2.5 m/s and a significant increase in the velocity gradient observed in the wall region, which is maintained up to 8 rotor diameters behind the wind turbine. The local increase in velocity

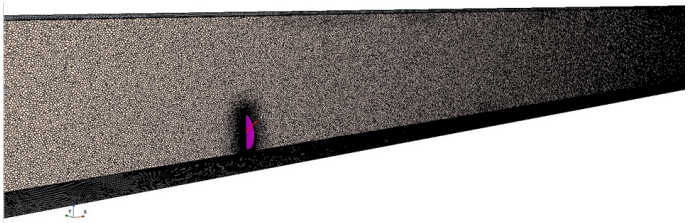

Figure 1: Wind tunnel with applied mesh and actuator disk

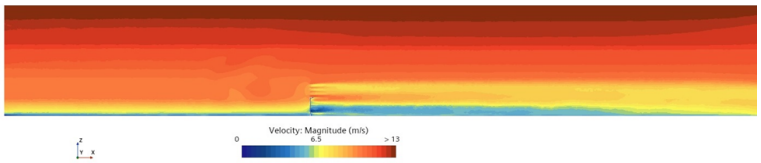

Figure 2: Velocity field of a single-phase wind flow around a single wind turbine

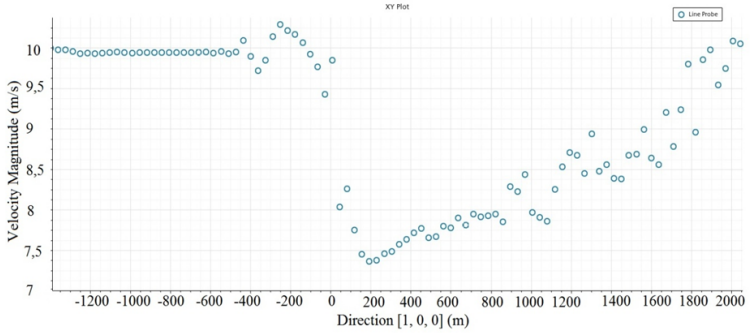

Figure 3: Velocity profile in the longitudinal axial plane-section of the wind tunnel at the hub level for single-phase flow

in the near wake region is explained by the peculiarities of the actuarial representation of the wind turbine in STAR CCM+. Fig. 3 shows the velocity profile in the longitudinal axial section of the design tunnel at the hub level for a single-phase flow.

As the results in Fig. 3 show, complete recovery of the air flow velocity without the dispersed phase is observed at a distance of 1900 meters behind the wind turbine.

The results of numerical studies the velocity fields in the presence of a dispersed phase simulating light and moderate rain are presented below. Fig. 4 shows the velocity field of a dispersed wind flow with a particle diameter $d = 1$ mm and the amount of precipitation per square meter 3,7 mm/h, characterizing light rain.

The near wake behind the actuator disk is characterized by a significant decrease in velocity, and the recovery of the flow in the far wake in the presence of a dispersed phase occurs more quickly. Fig. 5 shows the velocity profile in the longitudinal axial plane-section of the wind tunnel at the hub level for a dispersed flow with a particle diameter of d = 1 mm and a flow rate of 3,7 mm/h.

The results show a complete recovery of the air flow velocity for a dispersed flow with a particle diameter of d = 1 mm and a flow rate of 3,7 mm/h at a distance of 1750 meters behind the wind turbine. The presence of a dispersed phase in the air flow leads to a more rapid recovery of the turbulent wake behind the wind turbine due to the entrainment of particles by the flow and a reduction in the energy of turbulent eddies.

Fig. 6 shows a scalar scene of the velocity magnitude of the turbulent wake of a wind turbine with a dispersed phase with a particle diameter of d = 2.5 mm and a flow rate of 5,3

mm/h (moderate rain).

Fig. 7 shows the velocity profile in the longitudinal axial plane-section of the wind tunnel at the hub level for a dispersed flow with a particle diameter of d = 2,5 mm and a flow rate of 5,3 mm/h.

Analyzing the results of a numerical study of a dispersed flow with a particle diameter d = 2,5 mm and the amount of precipitation per square meter 5,3 mm/h full recovery of air flow

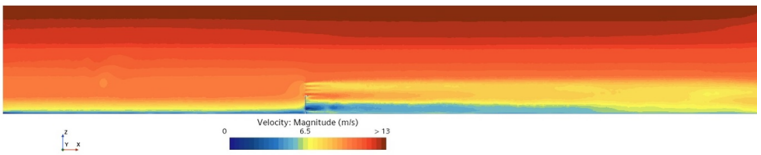

Figure 4: The velocity field of a dispersed wind flow with a particle diameter of d = 1 mm and a precipitation amount per square meter of 3,7 mm/h (light rain)

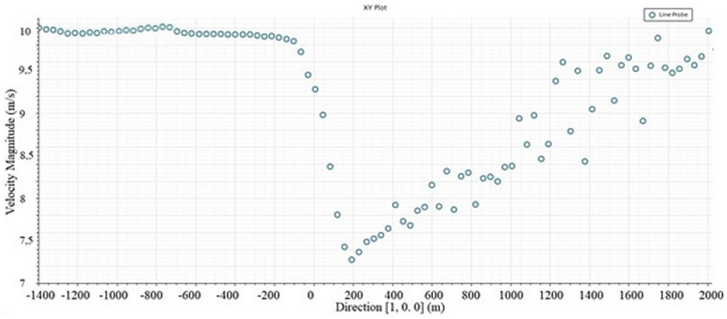

Figure 5: Velocity profile in the longitudinal axial plane-section of the wind tunnel at the hub level for a dispersed flow with a particle diameter of d = 1 mm and a flow rate of 3,7 mm/h (light rain)

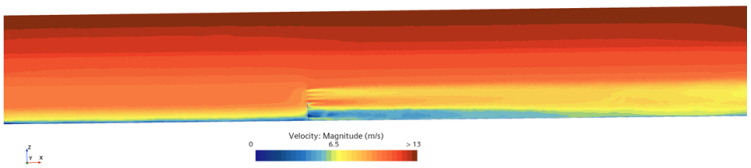

Figure 6: The velocity field of a dispersed wind flow with a particle diameter of d = 2,5 mm and a precipitation amount per square meter of 5,3 mm/h (moderate rain)

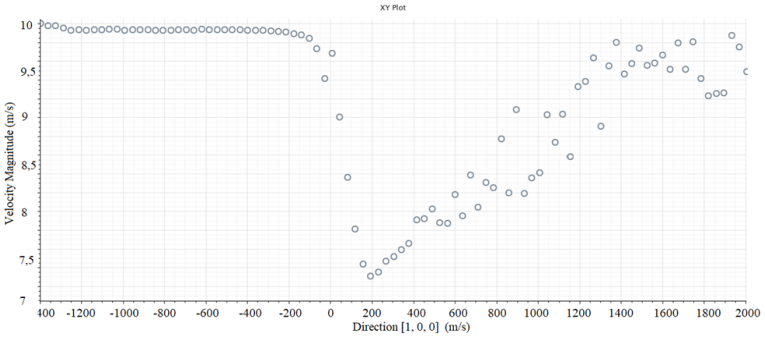

Figure 7: Velocity profile in the longitudinal axial plane-section of the wind tunnel at the hub level for a dispersed flow with a particle diameter of d = 2,5 mm and a precipitation amount per square meter of 5,3 mm/h (moderate rain)

velocity is observed at a distance of 1400 m behind the wind turbine. Research shows that the boundary layer recovery behind a wind turbine in the presence of a dispersed phase occurs faster due to the particles being drawn into the flow and the energy of turbulent vortices being reduced. Such results are related to the inertia of the particles [24].

5 Conclusions

The paper presents the results of a numerical study of the atmospheric boundary layer in the region of a wind turbine in the presence of a dispersed phase simulating precipitation. The study was performed using the CFD package STAR-CCM+ Academic Pack. The article notes that complete recovery of the air flow velocity without a dispersed phase is observed at a distance of 1900 m behind the wind turbine under the conditions under consideration. For a dispersed flow with a particle diameter of $d = 1$ mm and a flow rate of 3,7 mm/h, the turbulent flow is restored at a distance of 1750 m behind the wind turbine. For a dispersed flow with a particle diameter of $d = 2{,}5$ mm and a precipitation amount per square meter of 5,3 mm/h, complete recovery of the air flow velocity is observed at a distance of 1400 m behind the wind turbine. The presence of a dispersed phase in the air flow leads to a more rapid recovery of the turbulent wake behind the wind turbine due to the particles delay by the flow and a reduction in the energy of turbulent eddies.

Acknowledgement

The study was supported by a grant from the Russian Science Foundation 22-19-00030, https://rscf.ru/project/22-19-00030/

References

[1] *GWEC Global Wind Report 2023* . https://gwec.net/globalwindreport2023/

[2] Bezrukikh P.P., *Wind energy. Reference and methodological manual.* Moscow, “Energia”, 2010.

[3] Corrigan R. D., DeMiglio R. D., *Effect of precipitation on wind turbine performance.* National Aeronautics and Space Administration Lewis Research Center, 1985, 86986

[4] Vermaa A.Sh., Castrob S.G.P., Jiangc Z. , Teuwen J.J.E., *Numerical investigation of rain droplet impact on offshore wind turbineblades under different rainfall conditions: A parametric study.* Composite structures. 241 (2020), 112096.

[5] Law H., Koutsos V., *Leading edge erosion of wind turbines: Effect of solid airborne particles and rain on operational wind farms.* Wind Energy, 23.10 (2020), 1955-1965.

[6] Baidya Roy S., Pacala S. W., Walko R.L., *an large wind farms affect local meteorology?*. Journal of Geophysical Research: Atmospheres, 109 (2004), 1-6.

[7] Gvozdyakov D.V., *Numerical modeling of the process of condensation of combustion products of natural fuels of thermal power plants in the atmosphere.* Tomsk, TPU, 2010.

[8] Kovalnogov N.N., *Boundary layer in flows with intense effects*, Ulyanovsk, 1996.

[9] Varaksin A.Yu., *Flow around bodies by dispersed gas flows*, TVT, 56.2 (2018), 282-305.

[10] Pakhomov M.A., Terekhov V.I., *Effect of droplet evaporation on gas turbulence and heat transfer during two-phase flow behind a sudden expansion of a pipe.* TVT, 54.3 (2016), 352.

[11] Pakhomov M.A., Terekhov V.I., *Flow structure in a non-isothermal swirling gas-droplet flow behind a sudden expansion of a pipe.* Izvestiya RAS, MZhG, 1 (2016), 69.

[12] Li W., Ma Y., Liu X., Desbrun M., *Efficient Kinetic Simulation of Two-Phase Flows.* ACM Transactions on Graphics, 41.4 (2022), 114.

[13] Zhao W., Wan D., Zhao S., *CFD simulation of two-phase flows past a surface-piercing circular cylinder.* ISOPE International Ocean and Polar Engineering Conference, 2020, 3107.

[14] Palhares P., Guirardello R., *Numerical Simulation of the Two-phase Flow Inside Bubble Columns in the Fully Developed Flow.* Chemical Engineering Transactions, 100 (2023), 313-318.

[15] Porte-Agel F., Wu Y.T., Lu H, Conzemius R.J., *Large-eddy simulation of atmospheric boundary layer flow through wind turbines and wind farms.* Journal of Wind Engineering and Industrial Aerodynamics, 99.4 (2011), 154-168.

[16] Starchenko R.V., Nuterman R.B., Danilkin E.A., *Numerical modeling of turbulent flows and admixture transport in street canyons.* Tomsk, Tomsk University Publishing House, 2015.

[17] Andersson B., *Computational Fluid Dynamics for Engineers.* Cambridge, Cambridge University Press, 2012.

[18] Germano M.A., *Dynamic subgrid-scaled dyviscosity model.* Physics of Fluids, 3 (1991), 1760-1765.

[19] Ghosal S.A., *Dynamic localization model for large eddy simulation of turbulent flows.* Journal of Fluid Mechanics, 286 (1995), 229-255.

[20] *Simcenter STAR-CCM+.* http://saec.ru

[21] Lilly D.K., *A proposed modification of the Germano subgrid-scale closure model.* Physics of Fluids (1992), 633-635.

[22] Bliznyuk O.G., Vlasova O.E., Gichuk A.V., Kozelkov A.S., Lyalyushkina I.V., *Numerical modeling of multiphase flows in the Euler approximation based on the SIMPLE method.* FSUE "RFNC-VNIIEF", Sarov, Nizhniy Novgorod region, 2020, 22-32.

[23] Fatahian H., Salarian H., Eshagh Nimvari M., Khaleghinia, J., *Numerical simulation of the effect of rain on aerodynamic performance and aeroacoustic mechanism of an airfoil via a two-phase flow approach.* SN Applied Sciences, 2.5 (2020), 867.

[24] Varaksin A.Yu., *Turbulent flows of gas with solid particles.*, Moscow, Fizmatlit, 2003.

V.N. Kovalnogov,
Ulyanovsk State Technical University,
32 Severny Venetz Street, 432027 Ulyanovsk, Russia,
Email: kvn@ulstu.ru,

R.V. Fedorov,
Ulyanovsk State Technical University,
32 Severny Venetz Street, 432027 Ulyanovsk, Russia,
Email: r.fedorov@ulstu.ru,

A.V. Chukalin,
Ulyanovsk State Technical University,
32 Severny Venetz Street, 432027 Ulyanovsk, Russia,
Email: chukalin.andrej@mail.ru,

D.A. Demidov,
Ulyanovsk State Technical University,
32 Severny Venetz Street, 432027 Ulyanovsk, Russia,
Email: d.demidov@ulstu.ru,

M.I. Kornilova,
Ulyanovsk State Technical University,
32 Severny Venetz Street, 432027 Ulyanovsk, Russia,
Email: masha.kornilova.1995@mail.ru,

Yu.A. Khakhalev,
Ulyanovsk State Technical University,
32 Severny Venetz Street, 432027 Ulyanovsk, Russi,
Email: ulstu-td-ua@mail.ru.

Received 14.08.2024, Accepted 02.10.2024